ELSEVIER

Sensors and Actuators B 87 (2002) 201–206

SENSORS AND ACTUATORS B CHEMICAL

www.elsevier.com/locate/sensorb

Dynamics of electro-wetting droplet transport

Hong Ren[a,*], Richard B. Fair[a], Michael G. Pollack[a], Edward J. Shaughnessy[b]

[a]*Department of Electrical and Computer Engineering, P.O. Box 90291, Duke University, Durham, NC 27708, USA*
[b]*Department of Mechanical Engineering and Materials Science, P.O. Box 90291, Duke University, Durham, NC 27708, USA*

Abstract

A model is formulated to describe the dynamics of electro-wetting-induced transport of liquid droplets. The velocity of droplet transport as a function of actuation voltage is derived. The operating parameters include the viscosity of the droplet and the medium through which it actuates, contact-line friction, system geometry, and surface tension. Numerical coefficients are extracted from experimental data to represent the effect of operating parameters on electro-wetting dynamics. The power dissipation of droplet transport is analyzed which reveals the key limiting factors for device operation as well the effect of scaling on device power requirements.

Keywords: Microfluidics; Electro-wetting; Actuation; Droplets; Transport dynamics

1. Introduction

Microfluidic devices based on electro-wetting actuation (EWA) of droplets has recently been proposed and demonstrated [1]. The basic design of an electro-wetting actuator consists of parallel glass plates spaced apart. The space between the glass plates is filled with a host medium, such as silicone oil or air, and polarizable or slightly conductive liquid droplets that are immiscible with the oil. The top plate is coated with a ground plate electrode covered with a thin layer of hydrophobic insulation. The bottom plate consists of a patterned array of individually addressable electrodes covered with a hydrophobic insulating layer to form individual capacitors with the top ground plate. The hydrophobic insulators on both plates decrease the wettability of the surface. Fig. 1 illustrates a cross-section of the structure.

The physical principle of droplet actuation is based on electrostatic control of the interfacial tension at the droplet/insulator interface. Droplets with diameters comparable to the dimensions of the bottom electrodes sit between the top and bottom plates, and are manipulated by voltage switching on the bottom electrodes. To guarantee liquid actuation, droplets must be large enough to bridge the space between adjacent pairs of bottom electrodes. The start of droplet motion occurs by applying voltage to an electrode adjacent to where a droplet resides while simultaneously deactivating the electrode beneath the droplet. The accumulation of charge in the overlap region of the liquid/insulator interface reduces the interfacial tension at this interface. Consequently, a surface tension gradient is created across the gap between adjacent electrodes that drives the motion of the droplet. The direction of transport is easily controlled by switching the voltage from one adjacent electrode in the array to another.

EWA of a droplet appears to be promising conceptually for scalable microfluidic systems in that actuation is electrically controlled, rapid, reversible and requires low power (<10 μW). Possible applications have been suggested by Jackel et al. [2], Wahizu [3] and Fair et al. [4]. Most essentially, the reconfigurability of an EWA device makes it applicable to a wide range of operations in the same physical design, thus, greatly simplifying the design and fabrication of microfluidic systems. However, a detailed theoretical characterization of the EWA device is still lacking. Knowledge of the dynamics of EWA is useful in predicting device performance when physical and geometrical properties vary to meet the requirements of different applications. Meanwhile, the relationship between device performance and the operating parameters is essential to determine the feasibility of a EWA device in potential applications. Furthermore, to take full advantage of the scaling of EWA, a model needs to be examined to derive the best scaling factors in terms of device performance.

* Corresponding author. Tel.: +1-919-660-5423; fax: +1-919-660-5293.
E-mail address: renh@ee.duke.edu (H. Ren).

0925-4005/02/$ – see front matter © 2002 Published by Elsevier Science B.V.
PII: S0925-4005(02)00223-X

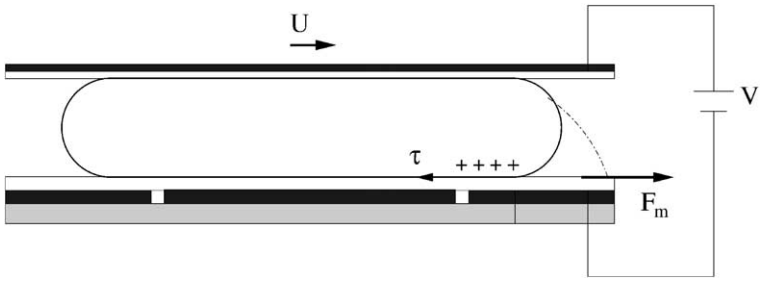

Fig. 1. Cross-section of an EWA device showing a droplet sandwiched between two glass plates. A voltage, *V*, is applied to an adjacent electrode, inducing charge in the overlap region. The reduction in liquid solid surface tension creates a surface tension gradient that pushes against the droplet, causing it to actuate to the right.

Finally, but not less importantly, knowledge of device dynamics helps in formulating a better understanding of the elements of power dissipation in EWA devices.

In this paper we analyze the dynamics of EWA devices, identify critical operating parameters, and discuss device performance with respect to power dissipation and dimensional scaling. The analysis reveals that viscous and physicochemical processes at the moving contact-line of the droplet are responsible for the bulk of mechanical energy dissipation, which in turn determines the dynamics of droplet transport. The results are supported by experimental data.

The work reported here is an extension of electro-wetting dynamics, whose principles were previously addressed by Beni and Tenan [5], and briefly mentioned by Prins et al. [6], and Lee et al. [7]. Beni, however, only considered the case where a liquid slug is pushed along a capillary tube by a continuous electrowetting effect. In the present work, we investigate a discrete droplet surrounded by a host medium where displacement is governed by a physicochemical contact-line wetting effect instead of by hydrodynamic principles. We adapt here an approach similar to that of Ruijter et al. [8] in analyzing droplet spreading by treating the droplet electro-wetting transport as a dissipative process. Combined wetting [9,10] and liquid displacement theories [11,12] have been applied to explain the phenomena of electro-wetting transport.

2. Modeling

A sketch of the generalized modeling approach is provided in Fig. 2. We consider a droplet sandwiched between two insulating surfaces separated by a gap and moving over insulated actuation electrodes. The diameter of the droplet, *D*, is comparable to the electrode pitch, *L*. Parameters of interest include the gap height between the glass plates, *h*, medium viscosity, μ_0, droplet viscosity, μ_d, and liquid medium interfacial tension, γ_{LM}. The principal assumption is that the liquid flow within the droplet can be approximated as laminar flow. This requires that the Reynolds number must be <1000:

$$Re = \frac{\rho UL}{\mu} \leq 1000 \tag{1}$$

where ρ, U, L, μ are the droplet density, average droplet velocity, length scale and viscosity, respectively. This condition is satisfied since the upper bound of droplet velocity is 10 cm/s for a pitch size of 1.5 mm. Thus, for an aqueous solution with viscosity around 1 cP, the Reynolds number

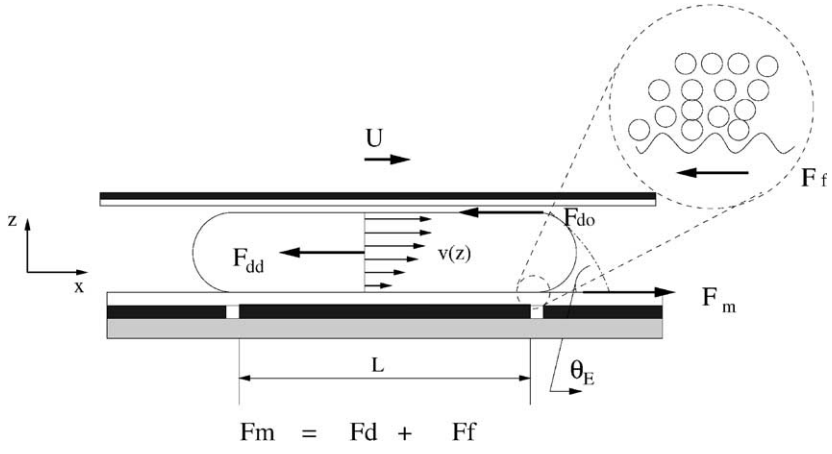

Fig. 2. 1D model of droplet transport showing sources of energy dissipation. F_m is the electrostatic driving force per unit length acting on the droplet, F_{dd} is a viscous flow force within the droplet, F_{do} is a viscous flow force in the oil medium, and F_f is the contact-line friction force. *U* is the average transport velocity.

does not exceed 100. To further simplify our analysis, another assumption is introduced to approximate the flow as quasi-steady-state flow. Finally, the capillary number considered in the study is on the order of 10^{-3} to 10^{-2}.

3. Droplet transport model

The steady-state transport model is developed based on the principle of balancing the work done by the external capillary force with the energy transformed and dissipated during droplet transport. The external force is caused by the difference in solid/liquid interfacial tension created at the interface between the droplet and the bottom insulator as a result of a difference in the voltage applied between adjacent electrodes. The components of energy dissipation are contributed by viscous flow within the droplet during transport, an oil viscous effect, oil resistance, as well as friction around the contact-line. The elements of the 1D model are illustrated in Fig. 2.

Laplace's equation was used to relate the difference in interfacial tension to the pressure differential developed across the front and back ends of the droplet. Then the external force can be expressed as a function of charge-induced reduction of surface tension, which in turn can be expressed in terms of electrostatic energy. Thus, the external force per unit length acting on the droplet, F_m, is equal to the electrostatic energy per unit area in Eq. (2). To take into account contact angle hysteresis between the front and back of the droplet and/or any other static friction, such as friction from adsorption, a threshold initiation force term, F_T, is added to represent the decrease in external force once transport is initiated.

$$F_m = \frac{\varepsilon_0 \varepsilon_R}{2d} V^2 - F_T \tag{2}$$

where ε_R is the permittivity of the bottom insulator and d is its thickness. It has been observed that the threshold voltage displays little variation with varying pitch sizes, gap heights, as well as viscosity. This may indicate that the droplet initiation force has little to do with fluid inertia or hydrodynamic friction. Rather, F_T is a function of the insulator surface's structure or is related to the surface's physical–chemical interaction with the liquid that could possibly be characterized by a static contact angle. In this study, an equivalent threshold voltage of 17 V was measured for water droplets of 100 mM KCL solution transported on a 1 μm Teflon AF1600.

The droplet viscous effect is demonstrated and modeled in this study by a stick-slip and/or jerky behavior at low and intermediate droplet transport velocities. It is believed that there is excess dissipation involved in the stick-slip contact-line motion, which can be better characterized hydrodynamically by solving the Navier–Stokes equation with a slip boundary imposed around the contact-line [12,13]. The corresponding viscous friction force is expressed as a function of capillary number ($C_a = \mu_d U/\gamma_{LM}$) and liquid-medium interfacial tension γ_{LM} in Eq. (3), where B is a fitting and dimensional coefficient.

$$F_d = B\left(\frac{\mu_d U}{\gamma_{LM}}\right)^{0.3} \gamma_{LM} \tag{3}$$

The capillary number is found to be related to the viscous friction force to the 0.3 power. This relationship was determined empirically by varying the droplet's viscosity and measuring its dependence on actuation voltage, while maintaining the same transport speed, U, and similar interfacial tension, γ_{LM}. The exponent coefficient 0.3 and numerical coefficient B are extracted by fitting Eq. (3) to the experiment data of Fig. 3 while relating the friction force with the external force in Eq. (2). $F_m = F_d + QU$, where QU is the term that is independent of the droplet viscous effect. Thus, the corresponding model and experimental droplet viscosity effects on transport are illustrated together in Fig. 3. The extracted coefficients are consistent with previously reported values [12], where the exponent of the capillary number was reported to be $0.45 \pm 0.1$and the numerical coefficient B was found to fall in the range $1 \leq B \leq 100$.

The mechanism by which the host oil medium retards the motion of the droplet's wetting line is still beyond current understanding. In this study, oil viscosity effects were analyzed and modeled to account for the large changes in actuation voltage by varying the oil viscosity.

Theoretically, it is known that oil with higher viscosity tends to be entrained more easily beneath the front edge of the wetting line [13]. The outward injected flow of entrained, displaced fluid will retard the wetting speed significantly. Meanwhile, in a horizontal-flow profile the stress generated on the oil-droplet interface causes a change in the curvature of the streamline near the boundary, leading to considerable energy dissipation. We expect the viscous stress caused by oil entrainment to be proportional to $\mu_0 U^*$ [12], where U^* is the local velocity profile around the contact-line. It is assumed that U^* is of the same magnitude as the average

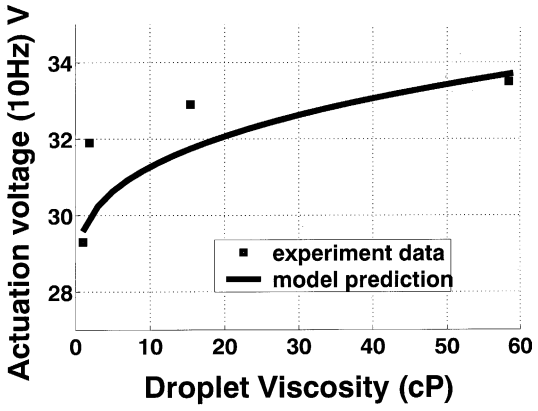

Fig. 3. Droplet viscosity effect on the actuation voltage required to transport a droplet at a constant velocity at an actuation frequency of 10 Hz. The curve fit to the data is based upon Eq. (3) and the results of [12].

droplet velocity, U. Similarly, since oil will flow around the droplet in a channel formed with the top ground plate, the viscous stress on the horizontal oil-droplet boundary will be proportional to $\mu_0 U$. We find that this viscous stress is loosely dependent on the aspect ratio of the electrode pitch to the plate spacing, L/h. We introduce adjustable coefficients that account for the oil viscous effect in the above two situations. Thus, an equation is derived to express the equivalent force per unit length to account for the effect of the oil:

$$F_0 = \left(\frac{mL}{h} + s\right)\mu_0 U \tag{4}$$

where adjustable coefficients 'm' and 's' are introduced into the expressions for viscous stress to account for oil entrainment and oil flow, respectively. The values for the coefficients (m, s) were determined by varying the oil viscosity and measuring the resulting effect on droplet actuation voltage. The coefficients 'm' and 's' are extracted by fitting Eq. (4) to the low velocity data of Fig. 4 while taking into consideration the geometry effect of oil viscous stress (data not shown). The resulting fitted model curve and the experimental droplet transport data are illustrated in Fig. 4.

Another dissipation effect proposed by Blake [14] is contributed by molecular adsorption and desorption processes around the contact-line. The theory states that there is a friction associated with the molecular displacement process around the contact-line, and at low velocity the friction force is linearly dependant on the velocity. Here, we make no attempt to evaluate this effect on theoretical grounds. However, it is suggested in the experimental data that at small and intermediate droplet velocities, there is an excess dissipation that could not be accounted for by viscous effects of the droplet and oil. Therefore, we simply include a linear contact-line friction effect in our model to represent the excess dissipation in small and intermediate velocity in this study.

$$F_f = \zeta U \tag{5}$$

Table 1
Extracted numerical coefficients from transport models

Threshold voltage (V)	17 ± 3
Droplet viscous effect (B)	0.55 ± 0.02
Oil viscous effect (m, s)	28 ± 3, 112 ± 10
Contact-line friction (ζ, dynes s/cm^2)	0.4 ± 0.02

where ζ is the contact-line friction coefficient in units of dynes s/cm^2. Thus, the equation that includes all the physically significant effects in EWA dynamics can be written as:

$$\frac{\varepsilon_0 \varepsilon_R}{2d} V^2 - F_T = B\left(\frac{\mu_d U}{\gamma_{LM}}\right)^{0.3} \gamma_{LM} + \left(\frac{mL}{h} + s\right)\mu_0 U + \zeta U \tag{6}$$

Subject to measurement variations of droplet velocities and controllability of the experimental conditions, the numerical coefficients were initially extracted by varying gap height, electrode pitch, oil viscosity, and droplet viscosity, and their values are reported in Table 1. Specially, the molecular friction factor, ζ, is extracted by fitting the small and intermediate velocity transport data in Fig. 5 to Eq. (6) with the droplet and oil viscous factors extracted with the process mentioned above.

Fig. 5 shows a comparison between a plot of Eq. (6) and data on droplet transport velocity versus actuation voltage for a 0.15 mm electrode pitch. The agreement is quite good using the extracted coefficients. Similar good results have been obtained with other system dimensions.

The basis for an analysis of the external force acting on a two-dimensional droplet is illustrated in Fig. 6. If the driving force per unit length is F_0, then the external force, F_m, is a function of droplet position as expressed in Eq. (7).

$$F_m = \int_{-\phi}^{\phi} F_0 \cos\phi \frac{L}{2} \, d\phi = LF_0 \sin\left(\arccos\left(1 - \frac{2x}{L}\right)\right) \tag{7}$$

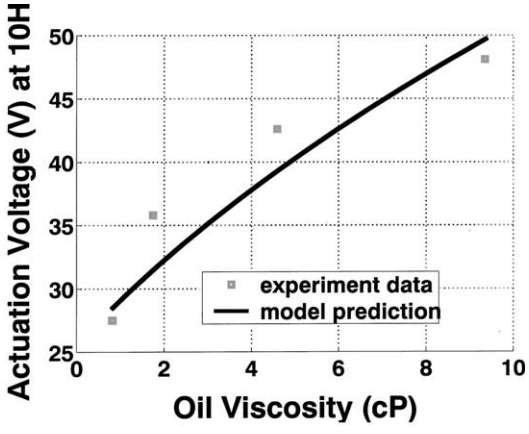

Fig. 4. Oil viscous effect on the actuation voltage necessary to maintain a constant droplet transport velocity at 10 Hz. The fitting curve is based on the representation of Eq. (4).

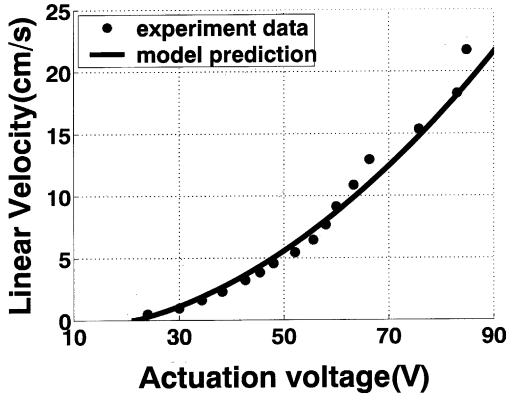

Fig. 5. Linear droplet velocity data vs. actuation voltage for transport over electrodes with a 0.15 mm pitch. The calculated curve is from Eq. (6) using the extracted coefficients in Table 1.

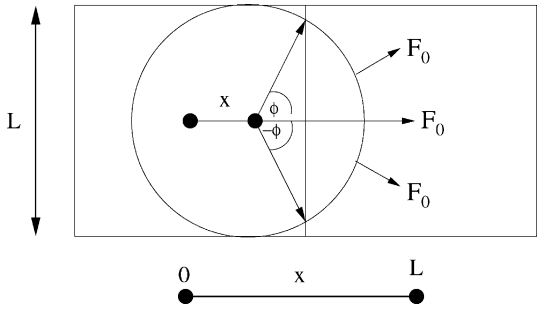

Fig. 6. Top view of droplet transport showing the varying external force. The droplet moves from an electrode to the left of an adjacent electrode to which a voltage is applied. F_0 is the driving force per unit length. The droplet diameter is assumed to be equal to the pitch size.

When averaging the driving force over the traveling distance, the external force is derived as:

$$F_{\text{ext}} = \frac{1}{L}\int_0^L F_{\text{m}}\,\mathrm{d}x = \left(\left(\frac{\varepsilon_0\varepsilon_{\text{R}}}{2d}\right)V^2 - F_{\text{T}}\right)\left(\frac{\pi L}{4}\right) \tag{8}$$

Inclusion of two-dimensional droplet and oil viscous effects as well as contact-line friction leads to the same result as shown in Eq. (6). Thus, the model is applicable to real droplet transport situations.

4. Power dissipation analysis

The power delivered to the droplet capacitor is calculated by considering the charging of the time-varying capacitance. Dynamic $C(t)$ curves were measured when a droplet was actuated onto an electrode. The time variation of capacitance is partially due to the droplet's time-dependent position over the electrode and partially due to oil entrainment [4]. The instantaneous power delivered to a time-varying capacitance $C(t)$ is:

$$P(t) = V^2\frac{\mathrm{d}C(t)}{\mathrm{d}t} \tag{9}$$

where V is the supply voltage. Assuming a linear change of capacitance over time, the average dynamic power delivered is $V^2C_{\text{f}}f$, where C_{f} is the final capacitance and f is the average transport frequency over the electrodes, such that $f = U/L$. Of the total dynamic power delivered, one-half is stored in an electrical form in the droplet capacitor as $1/2V^2C_{\text{f}}f$, and another half is dissipated through a combination of viscous, inertial and chemical processes in the EWA device. Of the total power loss, the part due to transport initiation is evident through the existence of a threshold voltage. Thus, the initiation loss is a considerable fraction of the total. For example, a 0.5 μl droplet of 100 mM KCl in silicone oil that is transferred between adjacent 1.5 mm pitch electrodes at 29 V and 10 Hz will dissipate 260 nW of power. The initiation static power constitutes about 200 nW or 77% of the total power. The rest of the work is partly done to generate the mechanical movement during which viscous and physical processes occur that are responsible for limiting and maintaining the average transport velocity. Our experimental observation that droplet transport is independent of the electrical conductivity of the liquid in the droplet eliminates the possibility of a dominant resistive dissipation, thus, further supporting our conclusions. Using the extracted numerical parameters, the distribution of power consumption beyond the initiation power is estimated in Table 2.

Table 2
Distribution of dynamic power consumption at 1.5 cm/s droplet transport velocity

Dynamic power (μW)	0.18
Contact-line (%)	59
Oil viscous (%)	27
Droplet viscous (%)	14

The data in Table 2 show that power dissipation due to contact-line friction is comparable to the combined viscous power dissipation contributions of the droplet and the oil medium together. This indicates that to increase the efficiency of droplet transport, attention should be paid to contact-line dissipation, which may limit the transport velocity, assuming we have control of other fluidic properties. For easily controlled properties, such as viscosity, our analysis shows that the oil medium viscosity also plays a dominant role in the droplet flow dynamics. Reducing oil viscosity will lead to a decrease of power dissipation. Droplet viscous dissipation, however, is less important compared to other factors. This is fortunate since it allows flexibility in the selection of actuated liquids. The transport initiation power is another factor that needs to be investigated, since it is the dominant factor in the range of small and intermediate transport velocities and it is the limiting factor in further decreasing the actuation voltage.

The power due to transport initiation is defined here as the *initiation power*, and the average power delivered to mechanical droplet transport is defined as *dynamic power*. The dynamic power is derived by multiplying the average external driving force over the traveling distance in Eq. (8) by the average transport velocity:

$$P_{\text{d}} = F_{\text{ext}}U = \left(\left(\frac{\varepsilon_0\varepsilon_{\text{R}}}{2d}\right)V^2 - F_{\text{T}}\right)\left(\frac{\pi LU}{4}\right) \tag{10}$$

where F_{ext} is the external driving force in Eq. (7). Similarly, the power consumed by transport initiation is derived as

$$P_{\text{s}} = F_{\text{T}}\left(\frac{\pi LU}{4}\right) \tag{11}$$

The initial power scales with the pitch size, L, or droplet size. This can be explained by the fact that droplet transport initiation is a function of the surface characteristics of the insulator, which in turn, are proportional to surface area (droplet size).

The total power dissipation, derived from the process of charging a time varying capacitor in Eq. (9) is the addition of

the initiation and dynamic power derived from two-dimensional droplet transport analysis:

$$P_t = \frac{1}{2}V^2 C_f f = \left(\frac{\varepsilon_0 \varepsilon_R}{2d}\right) V^2 \left(\frac{\pi L U}{4}\right) \quad (12)$$

5. Conclusions

The major result of the paper is contained in Eq. (6) that yields the velocity of droplet transport as a function of actuation voltage and relevant physical parameters. Table 2 that reveals the contributions of power dissipation in EWA. The physical parameters include viscosity, contact-line friction, geometric factors, and surface tension.

The existence of an oil medium is revealed to decrease the contact angle hysteresis, thus, decreasing the threshold voltage. However, at the same time the oil contributes considerably (around 30%) to dynamic power dissipation in the transport process. As a result there will be a trade-off between the benefits of the oil medium and transport performance.

Contact-line friction contributed by surface absorption can be substantial. For simple aqueous solutions in oil, around 60% of the dynamic power is consumed by this effect. Empirically, it has become clear that friction is dependant on contact angle. To guarantee EWA for certain liquids, the static and dynamic contact angles need to be examined carefully before applying EWA.

Droplet viscous effects are revealed to be less important in total dynamic power dissipation. However, when the capillary number exceeds a certain range, the droplet transport mechanisms proposed here may no longer be valid.

Acknowledgements

This work was supported under a grant from DARPA's Composite CAD Program.

References

[1] M.G. Pollack, R.B. Fair, A. Shenderov, Electrowetting-based actuation of liquid droplets for microfluidic applications, Appl. Phys. Lett. 77 (2000) 1725.
[2] J.L. Jackel, S. Hackwood, J.J. Veselka, G. Beni, Electrowetting switch for multimode optical fibers, Appl. Opt. 22 (1983) 1765.
[3] M. Wahizu, Electrostatic actuation of liquid droplets for microreactor applications, IEEE Trans. Ind. Appl. 34 (1998) 732.
[4] R.B. Fair, M.G. Pollack, R. Woo, V.K. Pamula, H. Ren, T. Zhang, J. Venkatraman, A microwatt metal-insulator-solution-transport (MIST) device for scalable digital bio-microfluidic systems technical digest, in: Proceedings of the IEEE International Electron Device Meeting, 2–5 December 2001, Washington, DC, USA.
[5] G. Beni, M.A. Tenan, Dynamics of electrowetting displays, J. Appl. Phys. 52 (1981) 6011.
[6] M.W.J. Prins, W.J.J. Welters, J.W. Weekamp, Fluid control in multichannel structures by electrocapillary pressure, Science 291 (2001) 277.
[7] J. Lee, H. Moon, J. Fowler, T. Schoellhammer, C.-J. Kim, Electrowetting and electrowetting-on-dielectric for microscale liquid handling, Sens. Actuators A 95 (2002) 259–268.
[8] M.J. De Ruijter, J. De Coninck, G. Oshamin, Droplet spreading: partial wetting regime revisited, Langmuir 15 (1999) 2209–2216.
[9] T.D. Blake, A. Clarke, E.H. Stattersfield, An investigation of electrostatic assist in dynamic wetting, Langmuir 16 (2000) 2928–2935.
[10] M. Vallet, M. Vallade, B. Berge, Limiting phenomena for the spreading of water on polymer filmes by electrowetting, Eur. Phys. J. B 11 (1999) 583–591.
[11] E.B. Dussan, Immiscible liquid displacement in a capillary tube: the moving contact line, AlChe J. 23 (1977) 131.
[12] M.-Y. Zhou, P. Sheng, Dynamics of immiscible-fluid displacement in a capillary tube, Phys. Rev. Lett. 64 (1990) 882.
[13] S.F. Kistler, Hydrodynamics of Wetting, in: Wettability, Surfactant Science Series, Vol. 49, Marcel Dekker, New York, 1993, pp. 311–429.
[14] T.D. Blake, Dynamic contact angles and wetting kinetics, in: Wettability, Surfactant Science Series, Vol. 49, Marcel Dekker, New York, 1993, pp. 251–309.

Biographies

Hong Ren, received MS in Electrical Engineering from Duke University in 2000, currently, she work toward PhD degree in Duke University. Her research interests include microfluidic, lab-on-chip, microsystem design, modeling and simulation, sensors interface design.

Richard B. Fair is professor of Electrical and Computer Engineering at Duke. He received the PhD from Duke University in 1969. He then spent 12 years at Bell Labs working on semiconductor devices and integrated circuit technology. He returned to North Carolina in 1981 and spent 13 years as an officer of MCNC, having responsibilities in chip design, computer-aided design, packaging, process technology, and MEMS. His current research interests include bio-MEMS and bio chips. He has published over 120 papers in refereed journals and conference proceedings, written 10 book chapters, edited eight books or conference proceedings, and given over 100 invited talks, mostly in the area of semiconductor devices or the fabrication thereof. Dr. Fair is also a Fellow of the Institute of Electrical and Electronic Engineers (IEEE), and Fellow of the Electrochemical Society, past Editor-in-Chief of the Proceedings of the IEEE, and he has served as Associate Editor of the IEEE Transactions on Electron Devices. He is a recipient of the IEEE Third Millennium Medal.

Michael G. Pollack received PhD degree in Electrical and Computer Engineering, Duke University, 2001. His research interests include microfluidics, and lab-on-a-chip technologies.

Edward J. Shaughnessy, is professor of Mechanical Engineering and Materials Science, Duke University. He received PhD degree in Aerospace Engineering, University of Virginia, 1975. His research interests include electrohydrodynamics, microfluidics, and particle filtration.